Experimental optomechanics with silicon micromirrors

Olivier Arcizet, C. Molinelli, T. Briant, P.-F. Cohadon, A. Heidmann, J.-M. Mackowski, Christine Michel, L. Pinard, O. Français, L. Rousseau

Experimental optomechanics with silicon micromirrors

O. Arcizet, C. Molinelli, T. Briant, P.-F. Cohadon, A. Heidmann

Laboratoire Kastler Brossel, ENS, CNRS, UPMC
Case 74, 4 place Jussieu, F75252 Paris Cedex 05, France

E-mail: cohadon@spectro.jussieu.fr

J.-M. Mackowski, C. Michel, L. Pinard

Laboratoire des Matériaux Avancés, Université Claude Bernard,
Bâtiment VIRGO, 22 Bd Niels Bohr, F69622 Villeurbanne Cedex, France

O. Français, L. Rousseau

ESIEE, ESYCOM, Université Paris-Est,
Cité Descartes BP 99, 2 Bd Blaise Pascal, F93162 Noisy le Grand Cedex, France

Abstract. We experimentally demonstrate the high-sensitivity optical monitoring of moving micromirrors, made of low-loss dielectric coatings upon silicon resonators of various shapes and sizes. The record optical finesses obtained ($\mathcal{F} \simeq 30\,000$) has allowed us to measure the thermal noise of the micromirrors at room temperature with a quantum-limited sensitivity at the $10^{-19}\,\mathrm{m}/\sqrt{\mathrm{Hz}}$ level and to completely characterize their mechanical behaviour, in excellent agreement with the results of a finite-element computation. Applications of such optomechanical systems range from quantum optics experiments to the experimental demonstration of the quantum ground state of a macroscopic mechanical resonator.

1. Introduction

Optomechanical systems, in which the intrinsic low-noise operation of optical measurements and moving mirrors yield very high-sensitivity displacement- or force-measurements, have been studied for over three decades in the framework of interferometric gravitational-wave detection [1, 2] and their ultimate quantum limits have been theoretically investigated [3, 4]. Such systems have also been considered to perform quantum optics experiments such as squeezing of the light field [5], QND measurements [6], or creation of non-classical states of the mirror motion [7, 8], even though very few experiments were actually performed [9, 10, 11], and always at a level far from the quantum domain.

Optomechanical systems have anyhow been central to world-record force-measurement in an optical AFM [12], and further progress with low- [13], medium-[14] or high-finesse optical cavities [15, 16, 17] as well as silica microtoroids [18], has allowed to enter a new regime where not only does the mirror motion impact the light field, but the coupling also acts the reverse way: back-action effect induced by the intracavity radiation field may for example cool the moving mirror.

In this article, we describe the high-sensitivity displacement monitoring of a silicon micromirror. The high finesse of the optical cavity, combined with the quantum-limited operation of the laser source and the detection system, has allowed us to monitor displacements at the level of $4 \times 10^{-19}\,\mathrm{m}/\sqrt{\mathrm{Hz}}$. This enables a careful comparison of the whole optomechanical behaviour of the micromirror with a finite-element modeling of the system. Sec. 2 is dedicated to a brief overview of the design, etching and optical coating of the micromirrors. In Sec. 3, we describe the optomechanical sensor, including the laser source and the optical detection setup we use throughout the paper. Sec. 4 is dedicated to the optomechanical characterization of the different vibration modes of the resonator, with a comparison to the results of a finite-element computation. In Sec. 5, we present further results which underline the multi-mode character of the resonator, summing up the single-mode results and using them to account for the observed wideband thermal noise spectrum of the micromirror. We also discuss the optomechanical characteristics obtained for a micromirror with a different geometry. We finally present a force-cancellation effect induced by the multi-mode behaviour of the micro-resonator, which is similar to the back-action cancellation mechanism recently observed for the radiation pressure exerted on a moving mirror [19].

2. Micro-resonator design and fabrication

Fabrication of the resonators proceeds as follows: we use $1\,\mathrm{cm}^2$ chips, cut in a 4-inch SOI wafer ($60\,\mu$m Si$||2\,\mu$m $SiO_2||500\,\mu$m Si), each with up to 4 micro-resonator structures. The structures are obtained by double-sided lithography and etched by Deep Reactive Ion Etching [20], in order to insure sharp edges. All resonators are $60\,\mu$m thick. The resonators under discussion in the following consist of $1\,\mathrm{mm} \times 1\,\mathrm{mm}$ (R1, see Fig. 1)

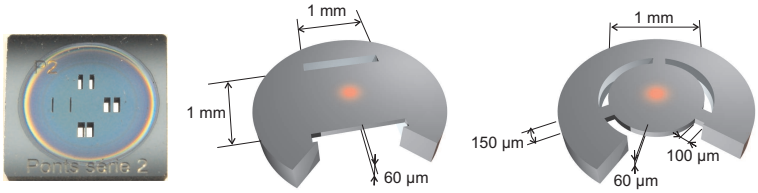

Figure 1. Left: Optical image of a chip with 4 micro-resonators (including R2 on the left). Center: Geometry of resonator R1. Right: Geometry of resonator R3. The red spot gives the relative size of the optical waist.

and 1 mm × 800 μm (R2) doubly-clamped beams, and a 1-mm triply-clamped disk (R3, see Fig. 1). With such dimensions, resonance frequencies are in the MHz range and the corresponding effective masses down to the μg level.

Each resonator chip is then cut and coated at the *Laboratoire des Matériaux Avancés* on the upper side with a very high-reflectivity and low-loss dielectric coating for 1064 nm. The micromirror is used as the back-mirror of an optical cavity. It is inserted in a mechanical structure which both guarantees optical parallelism and allows for its accurate transverse translation in order to provide a fine centering of the resonator and an optimization of its optomechanical behaviour. The input mirror has a 5 cm curvature radius, a transmission of 100 ppm, and losses of the order of 10 ppm. In order to lower the frequency noise, the cavity length is 2.4 mm, yielding an optical waist of 60 μm at the micromirror. The optical finesse of the cavity is deduced from the measurement of its bandwidth. The low roughness of the SOI substrate, together with the high quality of the optical coating, has allowed us to obtain very high optical finesses, up to $\mathcal{F} = 30\,000$, with typical overall losses (residual transmission and losses of the micro-resonator) on the order of 100 ppm.

The whole cavity is set inside a vacuum chamber, in order to immune it from acoustic perturbations, to lower the optical index fluctuations, and to increase the mechanical quality factors (see Sec. 4.5). The cavity is temperature-stabilized around room temperature with residual fluctuations below 10 mK.

3. Optomechanical sensing

The optical sensor is based upon a highly-stabilized Nd:YaG laser working at $\lambda = 1064$ nm (Fig. 2). The laser beam is sent through a wide-band electro-optic modulator (EOM) used as an intensity-modulation device, and a triangular spatial filtering cavity, locked onto resonance with the tilt-locking technique [21]. Our laser source therefore delivers a nearly perfect TEM_{00} gaussian mode with well-defined intensity and wavelength, and mode-matched to the high-finesse cavity by focussing lenses.

The laser frequency is locked at resonance by the Pound-Drever-Hall (PDH) technique via a resonant electro-optical modulator which provides a phase modulation of the incident beam at the sideband frequency of 12 MHz. The resonator displacements are monitored by the high-frequency part of the PDH error signal, and the displacements

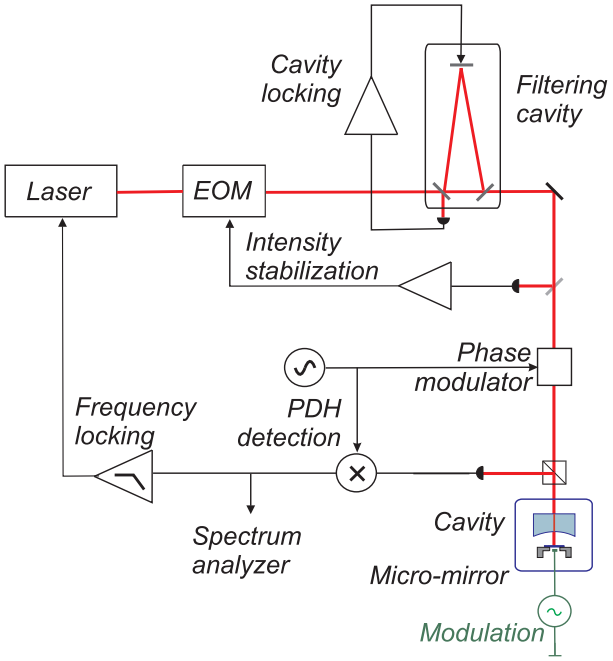

Figure 2. Experimental setup used to monitor the displacements of the micro-mechanical oscillator. A Nd:YAG laser beam (red) is intensity-stabilized with an electro-optic modulator (EOM) and spatially filtered before entering the resonator cavity. The displacement signal is extracted by means of a Pound-Drever-Hall phase modulation scheme using a resonant electro-optic phase modulator. The low-frequency part of the signal is used to lock the laser frequency to the cavity resonance. A voltage modulation applied to a metallic tip in the vicinity of the resonator allows to further check its mechanical behaviour.

are calibrated by comparison with the effect of a frequency modulation of the laser beam [9, 15].

Curves *b* and *c* of Fig. 3 represent relevant noises. Optical index fluctuations are irrelevant once the optical cavity is operated in vacuum. The frequency noise of the laser has been independently characterized with the filtering cavity: curve *b* presents an overestimated envelope. Frequency noise does not affect the sensitivity of our experiment for frequencies higher than 1 MHz: the sensitivity is then only limited by the quantum phase noise of the reflected field (curve *c*) to a level of $4 \times 10^{-19}\,\mathrm{m}/\sqrt{\mathrm{Hz}}$ at 1 MHz, in excellent agreement with the expected level, once taking into account every detail and imperfection of the optical setup.

4. Single-mode optomechanical characterization

4.1. Finite-element computation of the resonator

As the mechanical parameters (resonance frequencies, effective masses...) of doubly-clamped beams only have exact expressions for certain limits of their shape factors, we have used a finite-element modeling (FEM) program (Comsol Multiphysics) to compute

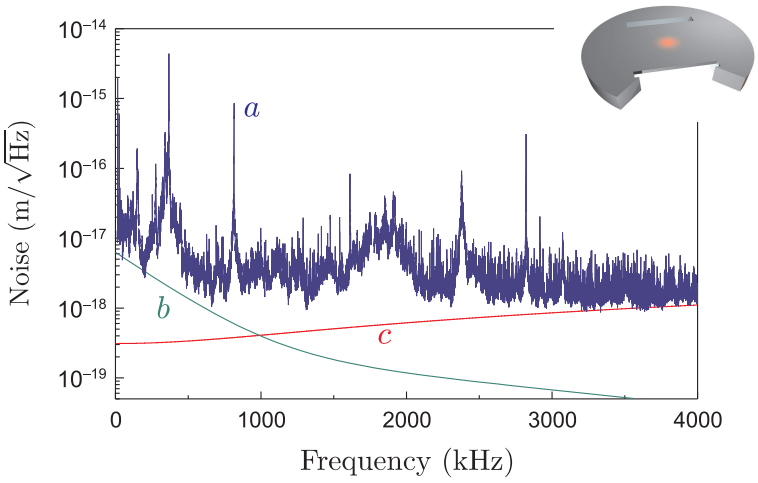

Figure 3. Thermal noise spectrum at room temperature, over a 4 MHz span (a), for resonator R1. Other curves represent relevant noise levels: overestimated frequency noise (b) and shot-noise (c).

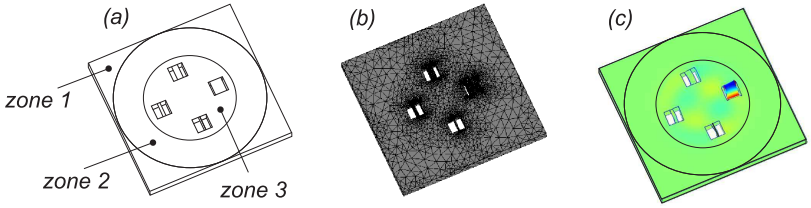

Figure 4. The three-step finite-element computation. (a) The geometry of the resonator and the mechanical constraints are defined. (b) The FEM program defines the mesh. (c) It computes the resonance frequencies along with the spatial profile of each vibration mode. Note the (low but finite) vibration amplitude at some vibration anti-nodes outside of the resonator.

the mechanical properties of the micromirrors.

Fig. 4 summarizes the three-step computation. The geometry of the micromirror is first defined. All the 1 cm^2 silicon chips are divided in three different zones. The silicon chip is firmly clamped on a brass piece on the front part of zone 1, whereas the back surface of both zones 1 and 2 is clamped to a copper piece. These constraints are given to the FEM program. Only zone 3, with up to four micromirrors, may freely move. The program then defines the required mesh, before computing the resonance frequencies and the corresponding vibration profiles, which enables to compute the stored elastic energy and therefore the effective mass of each mode.

For doubly-clamped beams (such as R1 and R2), the modes have a rectangular symmetry and can be indexed by two integers (p, q), each equal to the number of modes in an orthogonal direction. We will mainly focus in the following on *pure transverse modes*, i.e. $(0, q)$ modes with limited vibration in the direction of the clamping (see

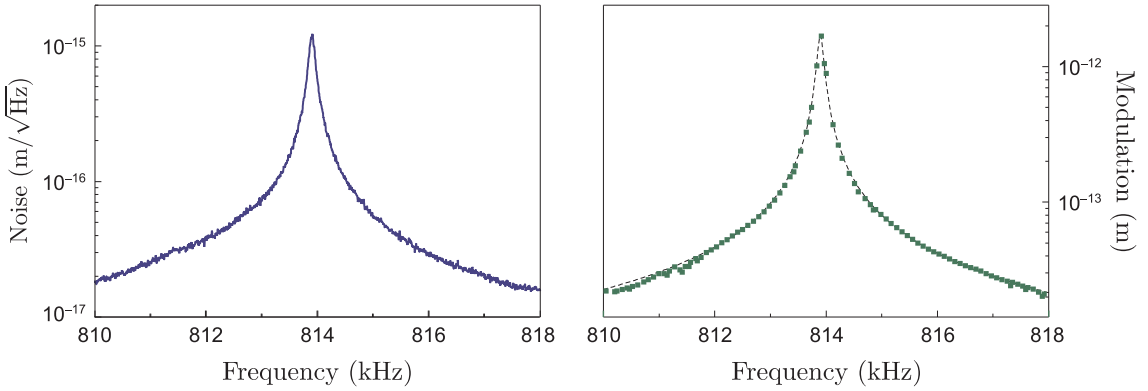

Figure 5. Left: thermal noise spectrum around the 814 kHz resonance of resonator R1, at room temperature. Right: mechanical response of the same mode to a modulated electrostatic force (squares) and corresponding lorentzian fit (dashed line).

Sec. 4.4). For disks (such as resonator R3), the modes can be as well indexed by two integers, one related to the radial symmetry, and one to the orthoradial one.

4.2. Experimental determination of the optomechanical parameters

Curve *a* of Fig. 3 presents the calibrated thermal noise spectrum obtained at room temperature, with a resolution bandwidth of 20 Hz and for an incident laser intensity of 1.5 mW. This spectrum exhibits sharp peaks with a high dynamics, which can be used to pinpoint the mechanical resonances of the micro-resonator.

The observed wideband thermal noise spectrum can be seen as the sum of thermal peaks and off-resonance tails of every vibration mode [22], which our setup allows to study in great detail. Left curve of Fig. 5 presents for instance the noise spectrum acquired over a 4 kHz span centered around the mechanical resonance at 814 kHz. A lorentzian fit of the resonance gives access to the optomechanical characteristics of the mode: resonance frequency $\Omega_{02}/2\pi \simeq 814\,\mathrm{kHz}$, effective mass $m_{02}^{\mathrm{eff}} \simeq 190\,\mu\mathrm{g}$, in good agreement with the expected values (890 kHz and 130 μg), computed with FEM.

Table 1 shows the measured resonance frequencies and effective masses, together with the FEM results and the measured mechanical quality factors for pure transverse $(0, q)$ modes as well as for the $(2, 2)$ one. In vacuum, the mechanical quality factors vary from a few thousands to 15 000.

The discrepancy between the measured and computed values of the resonance frequency decreases quickly and is below 5% for higher pure transverse modes. It appears to be mainly due to the coupling of the resonator modes with the wafer modes, as show both the dependence of the computed frequencies with the location of the resonator over the chip and the remaining discrepancy for longitudinal modes such as $(2, 2)$.

The agreement between measured and computed effective masses is quite satisfactory for even transverse modes. For odd modes, the displacement vanishes at the center and the effective mass should be infinite: the finite effective masses measured are due to an off-centering of the resonator with respect to the optical axis of the cavity,

Mode (p,q)	$\Omega_{pq}/2\pi$ (kHz) measured	$\Omega_{pq}/2\pi$ (kHz) computed	Q_{pq} measured	$m_{pq}^{\rm eff}$ (μg) measured	$m_{pq}^{\rm eff}$ (μg) computed
(0,0)	367	436	6 000	101	148
(0,1)	477	525	500	350 000	330 000
(0,2)	814	893	10 000	197	130
(0,3)	1 612	1 659	10 000	6 000	5 000
(0,4)	2 824	2 822	15 000	210	203
(0,5)	4 366	4 365	15 000	8 000	5 000
(2,2)	2 384	2 798	3 000	464	470

Table 1. Comparison between the measured and computed mechanical parameters (resonance frequency $\Omega_{pq}/2\pi$ and effective mass $m_{pq}^{\rm eff}$), and measured quality factors Q_{pq} of a few vibration modes of resonator R1.

which is not known accurately. Computed values -typically a factor 1000 larger than for even modes- are determined with an off-centering of 5 μm, which accounts quite well for the experimental data.

4.3. Electrostatic actuation

In order to confirm which of the observed peaks are related to a mechanical resonance of the silicon micromirror, we have implemented an electrostatic actuation of the resonator. It consists of a voltage modulation applied to a metallic tip close to the back surface of the resonator. The metallic tip is positioned with a 3-axis translation stage, its transverse position being optimized by monitoring it on a CCD camera set behind the optical cavity.

A quick order-of-magnitude estimate of the electrostatic force yields a force of the order of 1 nN for a few Volts modulation. Taking into account the expected resonance frequencies and effective masses, this corresponds to displacements on the order of 10^{-12} m at the resonance frequencies: the thermal noise level ($10^{-15}\,{\rm m}/\sqrt{\rm Hz}$) is therefore quite negligible as long as the measurement bandwidth is small enough (usually in the 10-Hz range).

As the electrostatic force is quadratic with respect to the applied voltage, the voltage can be either modulated at half-frequency or applied together with a DC voltage. In both cases, the corresponding DC displacement is compensated by the frequency-locking of the laser to the moving mirror cavity. We have mainly used the latter mechanism, using the DC offset as a variable modulation depth.

The right curve of Fig. 5 shows the observed mechanical response as the actuation frequency is swept around the resonance frequency, along with the corresponding lorentzian fit. It confirms the mechanical origin of the resonance peak and the values of the resonance frequency $\Omega_{02}/2\pi$ and mechanical quality factor Q_{02}. It also yields an estimate of the effective mass $m_{02}^{\rm eff}$ in good agreement with the measured value, as far

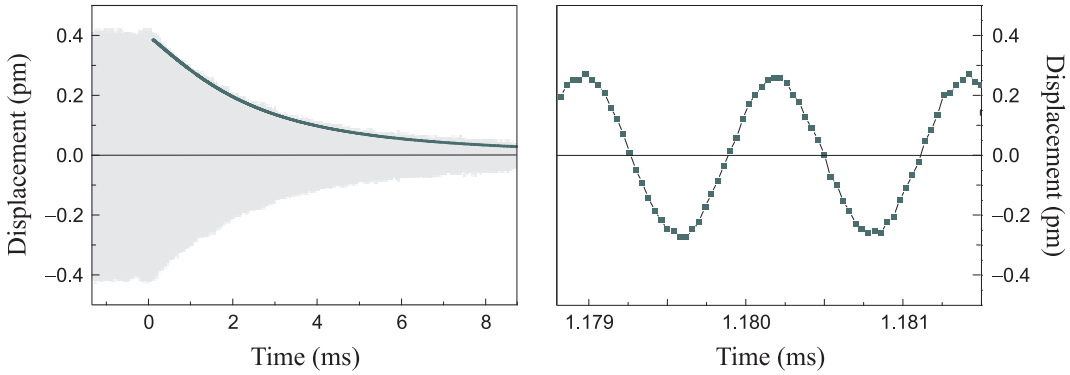

Figure 6. Decay of the modulated displacement once the electrostatic actuation is turned off (at $t = 0$). The right curve is a close-up of the left one, and displays the remaining oscillations. The vibration mode under study is the $(0, 2)$ mode of resonator R2 at 919 kHz.

as the electrostatic force exerted on the micromirror can be accurately calculated.

We have checked the linearity of the observed mechanical response with respect to both the DC and AC voltages. We have also checked the dependence of the force with the tip-resonator distance. For distances in the 50-300 μm range, when the tip is surrounded by the silicon substrate, we find the expected dependence for a sphere-plate system. For larger distances, the force no longer obeys that simple law, as the applied voltage can be electrostatically screened by the silicon wafer. In the following, the distance is set at 200 μm, which insures a large electrostatic force.

We have also taken advantage of this electrostatic actuation setup to further check the quality factor of the mechanical resonances. Once the resonator is driven into motion, we switch the modulation off and monitor the slow decay of the modulated displacement. Fig. 6 shows both the decay of the vibration envelope and a detail of the modulated displacement for the $(0, 2)$ mode (at 919 kHz) of resonator R2. The measured time constant of this decay is $\tau = 2.36$ ms, yielding a mechanical quality factor of 6 800, in excellent agreement with the 6 900 value deduced from the thermal noise spectrum.

4.4. Spatial profiles

The spatial profile can be mapped by translating a point-like actuation along the resonator surface while monitoring the amplitude of the response, as performed with radiation pressure actuation of larger fused silica mirrors [23]. Taking into account the small size of the resonator as well as the intrinsic long range feature of the electrostatic force, we have used a different approach: as the observed displacements depend on the overlap between the spatial structure of the mode and the optical intensity profile inside the cavity [23], the spatial profile is mapped by translating the resonator with respect to the laser beam while monitoring the level of the thermal noise at the mechanical resonance frequency. Fig. 7 presents the measured thermal noise level of the different modes of resonator R1, as a function of the transverse displacement between the

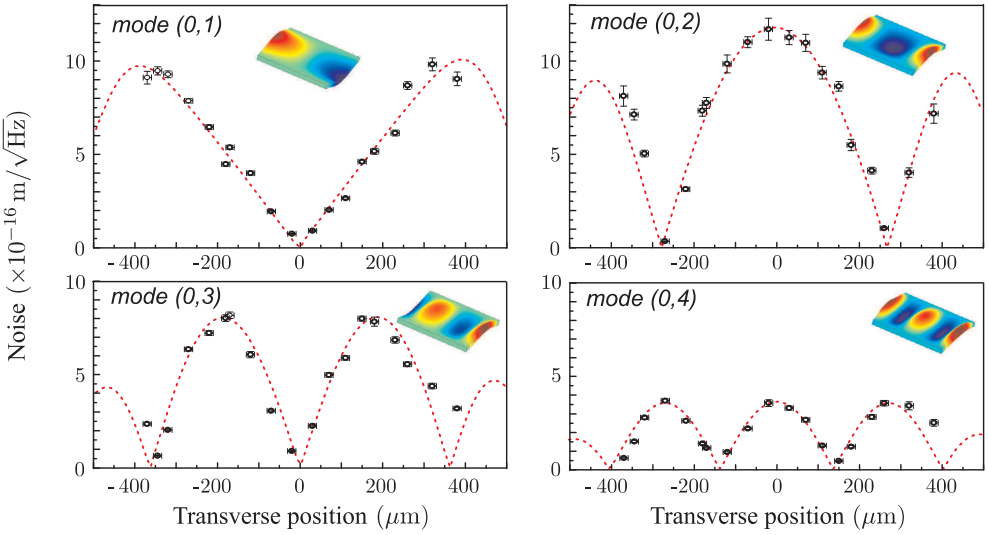

Figure 7. Variations of the thermal noise level as a function of the lateral position of the optical spot, for various vibration modes of resonator R1. Dots: experimental points; dotted line: fit with the expected spatial profile. The vertical error bars are mainly due to the optical finesse variation, especially at the edge of the resonator. Inserts show the corresponding computed spatial profiles.

resonator and the laser beam. The results are in excellent agreement with the noise levels expected from the computed spatial structure of the modes.

4.5. Mechanical quality factor

The mechanical quality factor Q is a very important feature for optomechanical experiments, as it concentrates the noise spectrum in the vicinity of the mechanical resonance. It therefore increases both thermal and quantum-mechanical noise levels at the resonance frequency, which may be of great help in the quest of the quantum ground state of the resonator, and lowers the same noise levels for out-of-resonance frequencies, thereby helping to experimentally demonstrate effects of radiation pressure in quantum optics experiments for instance. This subsection is devoted to an analysis of the variation of Q with respect to the surrounding pressure.

The quality factors are experimentally deduced from the widths $\Gamma_{pq} = \Omega_{pq}/Q_{pq}$ of the thermal noise spectra. Left curves of Fig. 8 show the observed pressure-dependence of the thermal noise spectrum of the $(0, 4)$ mode of resonator R1. As the pressure is varied in the vacuum tank, the optical length of the cavity changes and the laser has to be locked on the new optical resonance frequency of the cavity. The mechanical damping $\Gamma_{04}/2\pi$ shifts from its ambient pressure value of 1 100 Hz to a value of 190 Hz at 10^{-3} mbar, corresponding to a quality factor of 15 000.

Different kinds of behaviour have been experimentally observed. The damping of the $(0, 2)$ mode appears to have a linear dependence with pressure P above 20 mbar (see $\circ$ in the right chart of Fig. 8), which can be explained by acoustic emission from

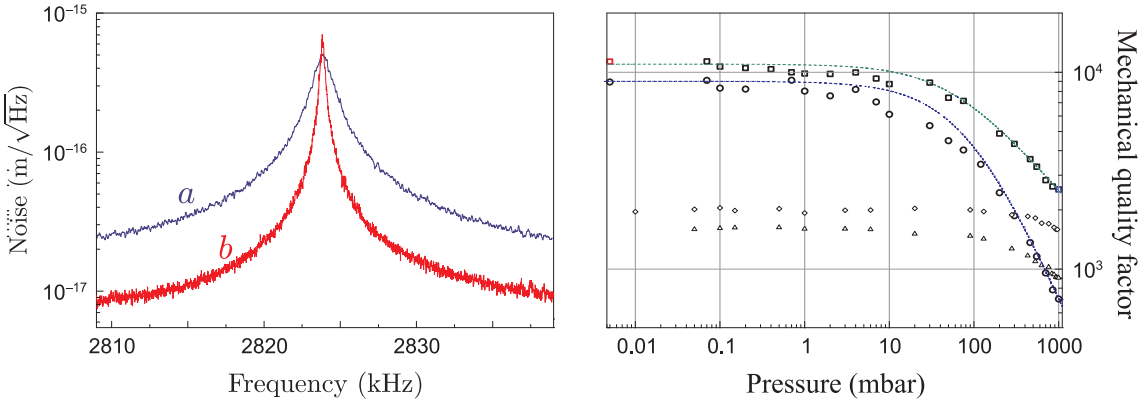

Figure 8. Left: thermal noise spectrum of the (0,4) mode of resonator R1, at ambient pressure (a) and in vacuum (b). The corresponding experimental points have the same color on the right chart. Right: dependence of the mechanical Q_{pq} factors for various modes of resonator R1 ($\circ$: (0,2) - $\diamond$: (0,3) - $\square$: (0,4) and $\triangle$: (0,5)), as a function of pressure. The green line represents a fit by a model with a viscous damping, whereas the blue line represents damping by acoustic emission.

the vibrating resonator (with lower pressure leading to lower acoustic emission and therefore lower losses). However, the $(0,4)$ mode obeys a different law: it appears to have a damping term proportional to $\sqrt{P}$ (see $\square$ in Fig. 8), which can be explained by the viscous damping of the resonator by the surrounding air. Other modes, such as $(0,3)$, have a too important damping constant at low pressure for any model to be tested on the limited pressure range experimentally available.

The mechanical damping appears to reach a minimum for pressures around and below 1 mbar. The corresponding value is somehow connected to clamping losses, as the highest values (up to 15 000) are obtained for pure transverse $(0,q)$ modes, with a low displacement at the clamping location [24]. Much higher values have however already been reported for resonators of similar dimensions or material [25, 26]. Such a discrepancy can be attributed to a number of reasons, including coating losses or coupling to the silicon chip, all of which still have to be investigated.

5. Multimode optomechanical behaviour

5.1. Multimode spectrum of resonator R1

Performing an individual study of each acoustic mode of the resonator allows us to quantitatively explain the observed multimode noise spectrum of Fig. 3. Curve b of Fig. 9 presents the thermal noise spectrum expected from the FEM simulation and the experimental optomechanical characterization: only modes predicted by the FEM were taken into account, with the experimental values (Ω_{pq}, m_{pq}^{eff}, Q_{pq}) obtained by fitting the individual thermal noise spectra, together with the quantum shot-noise.

The remaining discrepancy between these two curves, around 1 200 or 1 800 kHz, can be mainly attributed to the coupling between the resonator modes and neighbouring

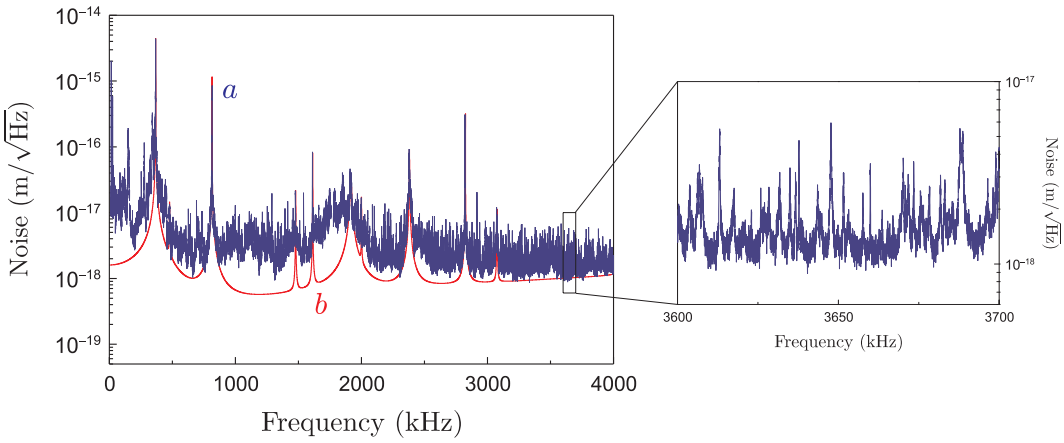

Figure 9. Left: experimental thermal noise spectrum of resonator R1, over a 4 MHz span (same as curve *a* of Fig. 3), and thermal noise spectrum expected from the FEM simulation and the single-mode characterizations (*b*). Right: zoom of the high-frequency part of the thermal noise spectrum, from 3.6 to 3.7 MHz, which exhibits a large number of small and thin peaks, probably related to vibration modes of the input mirror.

modes of the silicon chip, as accounted for by a noise spectrum monitored with the optical beam reflected upon the silicon wafer, but outside the resonator, which clearly exhibits the same vibration modes.

The number of smaller peaks which constitute a quasi-continuum at higher frequency (see right curve in Fig. 9) can probably be related to the modes of the input fused silica mirror, which is expected to have a comparable density of modes in this frequency range.

5.2. Multimode spectrum of resonator R3

In order to discuss the impact of the suspension of the system over its overall optomechanical features (as attested by the faint vibration amplitudes displayed outside the resonator on the theoretical vibration profile of resonator R1 on Fig. 4), we now turn to the thermal noise spectrum of resonator R3, displayed on Fig. 10.

The first significant vibration mode -at 272 kHz- is mainly a vibration mode of the loaded clampings, with the central resonator moving almost as a whole, without any major internal strain. Other modes (corresponding to the upper inserts if Fig. 10) are vibrations modes of the main resonator, with a low vibration amplitude at the clamping level, and a 3-fold symmetry due to the clamping geometry. Their effective masses are of the order of the mass of the resonator. The quality factors of such modes are notably enhanced by the suspension, up to a factor 4 with respect to a disk of similar dimensions but fully clamped over its border.

The spectrum finally displays highly-coupled modes of both the resonator and the suspension clampings. All experimental resonance frequencies are in excellent agreement (with relative discrepancy below 5%) with a FEM model of the resonator and its

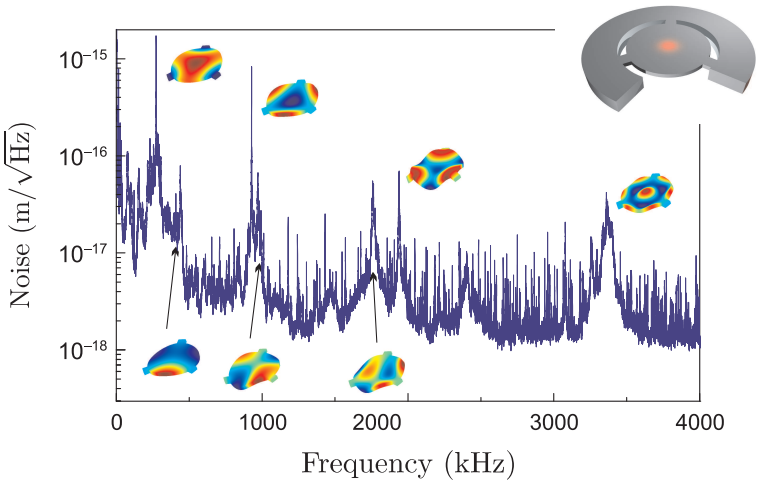

Figure 10. Thermal noise spectrum of resonator R3, at room temperature. Inserts show the vibration profiles of a number of significant vibration modes.

suspension design. The intrinsic angular degeneracy of the bare disk-shaped resonator is only slightly lifted by the 3-fold symmetry of the suspension, yielding the experimental observation of very broad (multi-mode) peaks in the noise spectrum.

The design of a resonator with a lower impact of the wafer upon its motion is currently under investigation.

5.3. Force cancellation

Up to now, the multi-mode optomechanical behaviour of the resonators can be seen as the sum of uncorrelated single-mode responses. We present in this subsection a different mechanism where the electrostatical actuation of the micromirror leads to a coherent excitation of both a resonant mode and the off-resonance mechanical response of all other vibration modes, leading to an effective cancellation of the mechanical response of the micromirror.

Fig. 11 presents the thermal noise spectrum of resonator R1 (curve *a*), in the vicinity of the $(0,4)$ resonance frequency. It can be fit (curve *b*) as:

$$S_x^T[\Omega] = \left| \frac{1}{m_{04}\left(\Omega_{04}^2 - \Omega^2 - i\Gamma_{04}\Omega\right)} \right|^2 S_T[\Omega] + S_0^T, \tag{1}$$

where $S_T[\Omega] = 2m_{04}\Gamma_{04}\Omega k_B T$ is the driving Langevin force and S_0^T the level of the background thermal noise, which we will assume frequency-independent in this frequency span. The fit yields the following optomechanical parameters: $m_{04} = 211\,\mu\text{g}$, $\Omega_{04}/2\pi = 2824\,\text{kHz}$, $\Gamma_{04}/2\pi = 1050\,\text{Hz}$ and $S_0^T = 4.0 \times 10^{-34}\,\text{m}^2/\text{Hz}$.

When driven by an external force characterized by a spectrum $S_F[\Omega]$, the modulation level can be fit as:

$$S_x^F[\Omega] = \left| \frac{1}{m_{04}\left(\Omega_{04}^2 - \Omega^2 - i\Gamma_{04}\Omega\right)} + \chi_0 \right|^2 S_F[\Omega], \tag{2}$$

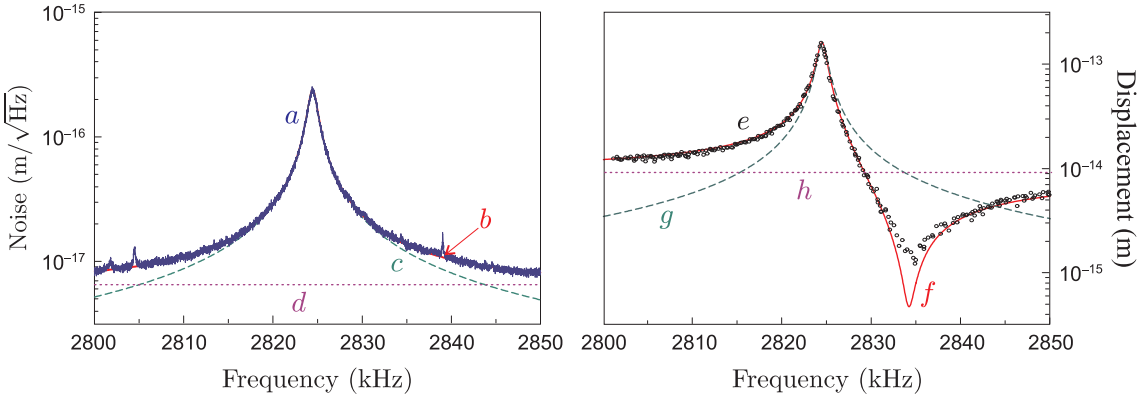

Figure 11. Thermal noise spectrum (a) and optomechanical response of the micromirror to an electrostatic force (e), in the vicinity of the $(0, 4)$ mechanical resonance at 2 824 kHz. Curves b and f display the theoretical fit (eqs. 1 and 2), with the contributions of both the resonant mode (c and g) and the off-resonance modes (d and h).

where χ_0 is the off-resonance mechanical susceptibility of all other vibration modes of the micromirror. χ_0 is real and positive as higher frequency modes (with a positive single-mode mechanical susceptibility $1/m_{pq}\Omega_{pq}^2$) have an overall higher contribution than the low-frequency ones (with $-1/m_{pq}\Omega^2$ contributions). As the driving frequency is swept across the $(0, 4)$ resonance frequency, the relative phase between the resonant and non-resonant terms therefore shifts from 0 to π: the mechanical responses accordingly either strengthen or cancel one another, leading to a dissymetrical mechanical response, including a cancellation of the response at a frequency slightly higher than the resonance frequency.

Fig. 11 presents the experimental results obtained with a modulated electrostatic force, which clearly exhibits a cancellation effect at a frequency slightly higher than the resonance frequency. The discrepancy around the cancellation frequency with the fit given by eq. (2) (curve f) may be due to electromagnetic interference signals. A related effect, in response to radiation pressure fluctuations, has already been experimentally demonstrated with a high-finesse optical cavity with twin fused silica mirrors [19] and might be used in a back-action evasion scheme in the context of the detection of gravitational-waves with resonant detectors [27].

6. Conclusion

We have presented an experiment where the motion of micromirrors is monitored at the $10^{-19}\,\mathrm{m}/\sqrt{\mathrm{Hz}}$ level with a stabilized laser source and a very high-finesse optical cavity. The motion and the optomechanical behavior have been fully studied and accounted for, both at and off-resonance, at frequencies of interest for quantum optics experiments. There is still room for improvement, both optical and mechanical: the cavity finesse achieved so far is mainly limited by the roughness of the commercial silicon wafer, and

higher values have already been obtained for the mechanical quality factor [26].

Low temperature operation of such a resonator opens the way to quantum optics experiments, as well as the experimental observation of the quantum ground state of a macroscopic mechanical resonator [28, 29]. A specific scheme, based upon radiation pressure cavity-cooling, has already been demonstrated [14, 16, 17, 18] and shown to allow for ground-state cooling [30, 31]. The single-mode resonant behavior observed over more than 40 dB with our resonator seems especially promising in that purpose. The knowledge of the other modes' dynamical behaviour indeed appears as a major issue on the road to the quantum ground state, as the out-of-resonance tails of other vibration modes will no longer be negligible compared to the resonant noise, and in fact already matter in our experiment [16] for extreme cooling ratios.

Acknowledgments

Acknowledgements are due to Francesco Marin and to Ping Koy Lam for providing us respectively with the input mirror of our measurement cavity and the mirrors of our filtering cavity, and to Vincent Loriette for the optical characterization of the micromirrors.

References

[1] C. Bradaschia *et al.*, Nucl. Instrum. Meth. A **289**, 518 (1990).
[2] B. Abbott *et al*, Phys. Rev. Lett. **95**, 221101 (2005).
[3] C. Caves, Phys. Rev. D **23**, 1693 (1981).
[4] M.T. Jaekel and S. Reynaud, Europhys. Lett. **13**, 301 (1990).
[5] C. Fabre, M. Pinard, S. Bourzeix, A. Heidmann, E. Giacobino, and S. Reynaud, Phys. Rev. A **49**, 1337 (1994).
[6] A. Heidmann, Y. Hadjar, and M. Pinard, Appl. Phys. B **64**, 173 (1997).
[7] S. Bose, K. Jacobs, and P.L. Knight, Phys. Rev. A **56**, 4175 (1997).
[8] M. Pinard, A. Dantan, D. Vitali, O. Arcizet, T. Briant, and A. Heidmann, Europhys. Lett. **72**, 747 (2005).
[9] Y. Hadjar, P. F. Cohadon, C. G. Aminoff, M. Pinard, and A. Heidmann, Europhys. Lett. **47**, 545 (1999).
[10] P.-F. Cohadon, A. Heidmann, and M. Pinard, Phys. Rev. Lett. **83**, 3174 (1999).
[11] I. Tittonen *et al.*, Phys. Rev. A **59**, 1038 (1999).
[12] D. Rugar, R. Budakian, H.J. Mamin, and B.W. Chui, Nature **430**, 329 (2004).
[13] C. Hohberger Metzger and K. Karrai, Nature **432**, 1002 (2004).
[14] S. Gigan *et al.*, Nature **444**, 67 (2006).
[15] O. Arcizet *et al.*, Phys. Rev. Lett. **97**, 133601 (2006).
[16] O. Arcizet, P.F. Cohadon, T. Briant, M. Pinard, and A. Heidmann, Nature **444**, 71 (2006).
[17] J.D. Thompson *et al.*, Nature **452**, 72 (2008).
[18] A. Schliesser, P. Del'Haye, N. Nooshi, K.J. Vahala, and T.J. Kippenberg, Phys. Rev. Lett. **97**, 243905 (2006).
[19] T. Caniard, P. Verlot, T. Briant, P.-F. Cohadon, and A. Heidmann, Phys. Rev. Lett. **99**, 110801 (2007).
[20] F. Marty *et al.*, Microelectronics Journal **36**, 673 (2005).
[21] D.A. Shaddock, M.B. Gray, and D.E. McClelland, Opt. Lett. **8**, 1499 (1999).

[22] P.R. Saulson, Phys. Rev. D **42**, 2437 (1990).
[23] T. Briant, P.-F. Cohadon, A. Heidmann, and M. Pinard, Phys. Rev. A **68**, 033823 (2003).
[24] M.C. Cross and R. Lifshitz, Phys. Rev. B **64**, 085324 (2001).
[25] B. Le Foulgoc *et al.*, J. Micromech. Microeng. **16**, S45 (2006).
[26] P. Mohanty *et al.*, Phys. Rev. B **66**, 085416 (2002).
[27] T. Briant *et al.*, Phys. Rev. D **67**, 102005 (2003).
[28] R.G. Knobel and A. N. Cleland, Nature **424**, 291 (2003).
[29] M.D. LaHaye, O. Buu, B. Camarota, and K.C. Schwab, Science **304**, 74 (2004).
[30] I. Wilson-Rae, N. Nooshi, W. Zwerger, and T.J. Kippenberg, Phys. Rev. Lett. **99**, 093901 (2007).
[31] F. Marquardt, J.P. Chen, A.A. Clerk, and S.M. Girvin, Phys. Rev. Lett. **99**, 093902 (2007).